International Journal of Physics and Applications

E-ISSN: 2664-7583
P-ISSN: 2664-7575
IJOS 2025; 7(1): 20-25
© 2025 IJPA
www.physicsjournal.in
Received: 13-11-2024
Accepted: 15-12-2024

G Thirumoorthi
PG & Research Department of Physics, Govt. Arts College (Autonomous), Salem-7, Tamil Nadu, India

R Anbarasan
PG & Research Department of Physics, Govt. Arts College (Autonomous), Salem-7, Tamil Nadu, India

B Gnanavel
PG & Research Department of Physics, Chikkaiah Naicker College, Erode-4, Tamil Nadu, India

Corresponding Author:
G Thirumoorthi
PG & Research Department of Physics, Govt. Arts College (Autonomous), Salem-7, Tamil Nadu, India

Nanoscale structural investigation of Magnesium (Mg) Doped Tungsten oxide (Wo_3) for Future photocatalytic applications

G Thirumoorthi, R Anbarasan and B Gnanavel

DOI: https://doi.org/10.33545/26647575.2025.v7.i1a.123

Abstract
Magnesium-doped tungsten oxide (Mg-WO_3) has emerged as a promising material for advanced photocatalytic applications due to its tuneable nanoscale properties and enhanced catalytic performance. In this study, Mg-WO_3 nanoparticles were synthesized via microwave irradiation method, and their structural, morphological, and optical properties were systematically investigated. The doping of magnesium into the WO_3 lattice was confirmed through X-ray diffraction (XRD) analysis, which indicated lattice distortion and a reduction in crystallite size due to Mg incorporation. Field emission scanning electron microscopy (FE-SEM) revealed a uniform nanostructured morphology with improved surface area, essential for catalytic activity. UV-visible spectroscopy demonstrated a significant bandgap narrowing, enhancing the material's ability to harness visible light effectively. Photocatalytic performance was evaluated using specific target pollutant or reaction with Mg-WO_3 exhibiting superior activity compared to pure WO_3. These findings highlight the potential of Mg-WO_3 nanostructures as efficient photocatalysts for environmental remediation and sustainable energy solutions.

Keywords: Tungsten oxide, microwave Irradiation, Mg doping

Introduction
Single Mg doping gives the most noteworthy IR transmission whereas single W doping presents the least IR transmission at diverse temperatures [1]. The temperature incline rate was 10 °C/min and was kept consistent over the distinctive runs [2]. Within the UV-NIR transmittance spectra, the assimilation edge moved somewhat to bigger wavelengths (red-shift) by including V dopant [3]. The temperature of dissolves is measured with a nickel-chromium thermocouple sheathed with an alumina tube [4]. Moreover, its special characteristics counting tall resistance to radiation at room temperature and moo development temperature are valuable for sundry applications [5]. The mean size of the Nano MgO Particles was between 80-120 nm [6]. The isomerization and the hydrogen scrambling responses of alkenes were moreover examined [7]. The primary top, due to an excitation move at appears solid temperature reliance and is settled as a doublet at 77°K [8]. The glass-based gadget did not appear the hydroxide state of nickel within the layer [9]. The reason for the separation was clarified through the multi slice picture recommending that the grid bungle between the clusters and the MgO grid was a key figure in deciding the picture differentiate [10]. At the same time, magnesium and tin are broadly utilized surface dynamic locales that can boost catalytic responses [11]. The sedimentation of Mg^{2+} was more positive almost 230 mV than that of other particles in electrolyte [12]. Tinning did not avoid the interaction between Mg and Al to create intermetallic compounds totally, but decreased the intermetallic compounds to a few degree [13]. A basic chemical statement method is received for this reason [14]. Silicon nitride displayed the most noteworthy resistance, appearing [15]. We watched that the terminal prepare of the decrease of Mg on a tungsten cathode is quasireversible [16]. Most of them are complicated and time-consuming, but for adsorption strategies, which are basic and helpful [17]. The strategy was adjusted for the assurance of palladium in natural tests [18]. As of late, bismuth has been utilized in solutions for the treatment of helicobacter pylori-induced gastritis 1, 2. Be that as it may, a number of poisonous impacts in people have been ascribed to bismuth compounds such as, nephropathy, hepatitis and neuropathology [19]. The source has been tried and characterized in a Nano Fab 150 cantered particle bar (Lie) framework [20].

Solidness of the gadget was assessed by cyclic exchanging test [21]. The test required to be dried at 100 °C for 10 min to enter the zinc shower [22]. For clear straightforwardness and solidness of the gadget, a composition of Mg-Ti lean film was optimized [23]. The thermodynamic information recommend that the spinel stage is entropy stabilized, and would be unsteady underneath (±25)°C at climatic weight [24]. Subsequently, the taken a toll of discuss conditioning and the resulting natural stack increment in summer [25]. On the other hand, moderately tall chemical dormancy of the rutile stage makes it a reasonable choice in applications where steadiness is basic [26]. On the opposite, liquid salt electrolysis is more favourable in terms of vitality utilization, labour efficiency and carbon dioxide gas outflows [27]. In moving toward higher efficiencies, it has long been recognized that major building or materials based adjustments are required [28]. Conventional strategies include collecting tests on area and after that transporting them to a research facility for examination, which is both time devouring and exorbitant. In this manner a reasonable, vigorous, convenient sensor that can precisely screen levels of poisonous quality is required [29]. They are presently broadly utilized within the areas of flying machine, car components, electronic communications, optical hardware, and versatile work force and computers [30]. Current showings of TIMDs have been constrained to either electrically inactive plans or remote controlling [31]. It has been detailed that EN plating has been carried out over Mg combinations utilizing tannic corrosive based transformation coating taken after by HF treatment [32]. Micro-hardness comes about affirm the change in mechanical properties of composites in nearness of WC support [33]. These perceptions demonstrated that post-treatment with suitable materials moves forward obstruction impacts of coatings determined by wet-chemical strategy [34]. Magnesium was kept on a nickel cathode from TC arrangements containing $Mg(FeCl_4)_2$ [35]. Separated from that, either the micro hardness of the creases, the extreme pliable quality, or the stretching of the welded joints was made strides by maturing treatment, whereas as well tall maturing temperature would allow rise to a strongly diminished extreme malleable quality [36]. Due to the biodegradability of Mg based embed materials, extra surgeries to expel inserts can be maintained a strategic distance from. Imperatively, the capacity to maintain a strategic distance from rehashed surgeries not as it were diminishes the horribleness rate of patients, but too comes about in diminished wellbeing care costs and abbreviated hospitalization [37]. Have arranged In-doped ZnO nanoparticles by sol-gel course and have examined their detecting reaction toward CO gas which is progressed compared to unadulterated ZnO. Other than, Mg doping was broadly examined much appreciated to its controllable band hole, less grid bungle with ZnO and great crystallinity [38]. The current-time profiles demonstrate a few impacts of electro-nucleation and -development [39]. The scraped spot resistance of nickel-tungsten (Ni-W) coatings depends not fair on their sturdiness but too on grain measurements.

Experimental details

Microwave illumination of hydrated tungsten oxide ($WO_3.H_2O$) nanoparticles at room temperature was utilized to incorporate both immaculate and doped nanoparticles [17]. For the try, we utilized 20 ml of sodium hydroxide to break down 4.98g of analytical-grade tungstic corrosive (H_2WO_4) (around one molar proportion) (NaOH). In encompassing circumstances, the coming about yellow arrangement was twirled for 20 minutes. A few of this may well be clarified by the proton trade method [18]. Magnesium Chloride ($MgCl_2$) and tungstic corrosive were at that point included to 20 ml of deionized water in arrange to make arrangement. A while later, the blend was carefully blended for another 20 minutes. This blend had an impartial pH (7.0) due to the salt substance, in this way HCl was included to bring the pH back down to one since it can accelerate the salts additionally offer assistance the ultimate item take on the specified morphology [19]. We at that point included 5 ml of double-distilled water (50 volume percent forerunner arrangement) to the previously mentioned arrangement so that it would react more rapidly to microwaves. The wrapped up arrangement of both immaculate and doped tests was exchanged to a microwave stove (2.45GHz and greatest control of 900 W) in encompassing settings and held at 600 W for 10 minutes. Destruction at 600 ^{0} C for six hours evacuated the sub products and moved forward crystallinity, coming about in a yellow accelerate.

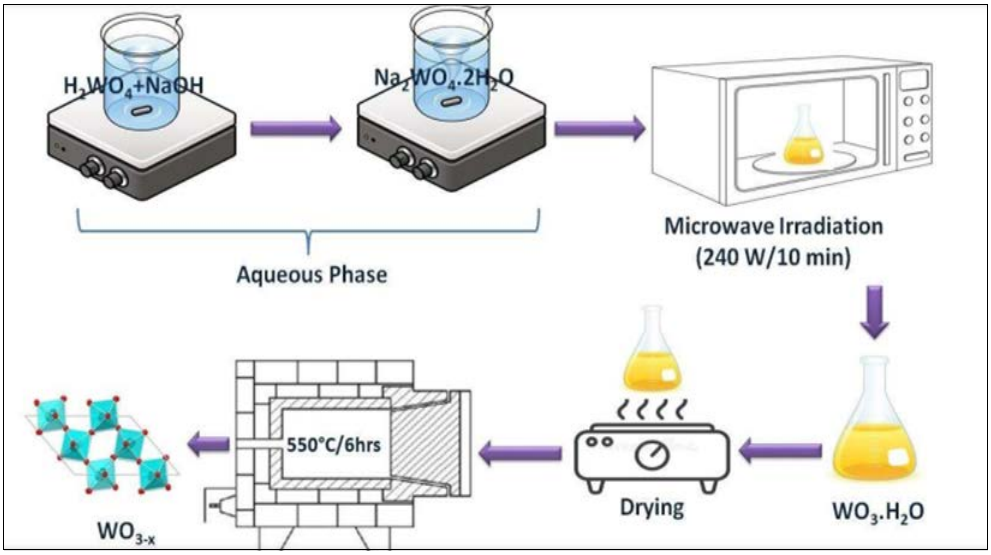

Fig 1: Schematic illustration of the synthesis of doped $WO_3.H_2O$ in a microwave atmosphere

Characterization

Powder XRD analysis

Figure 2 appears the powder XRD design for doped hydrated tungsten oxide, while Figure 3 appears the design for the comparing tempered tests (Figs. 2 and 3). For comparison, earlier ponders have portrayed in detail the powder XRD designs of WO_3- H_2O and WO_3- tempered. Agreeing to JCPDS reference number 43-0679, Powder XRD discoveries approved the orthorhombic stage improvement of WO_3- H_2O with an upgraded crystalline character. Note that the doped (0.02) sample's small move within the lower Bragg point side recommends the integration of dopant particles into the $WO_3.H_2O$ crystallinity through the utilize of dopant-ion molecules with huge orbital radii. For manganese (5 Wt.%), be that as it may, the re-achievement of crystallite location close Bragg's esteem of immaculate test along (020) plane taken after the joining of Mg particle into WO_2- (020) tetrahedron structure, not in water atom location (111), which is another affirmation of the achievement of the initial parent stage nature.

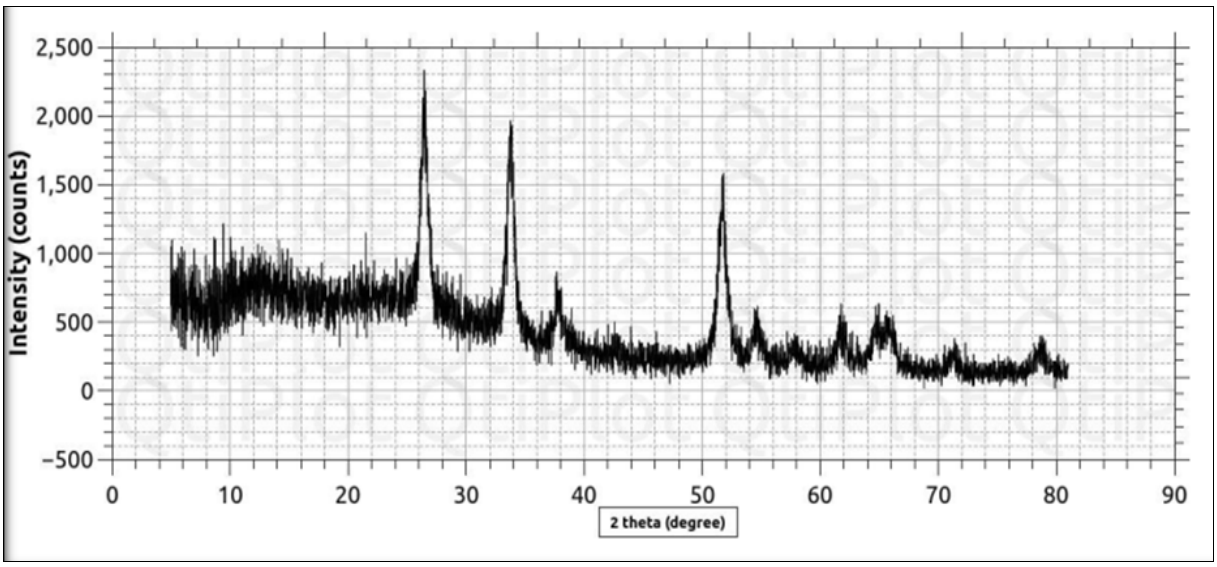

Fig. 2: Representative Powder XRD pattern of doped WO_3. H_2O

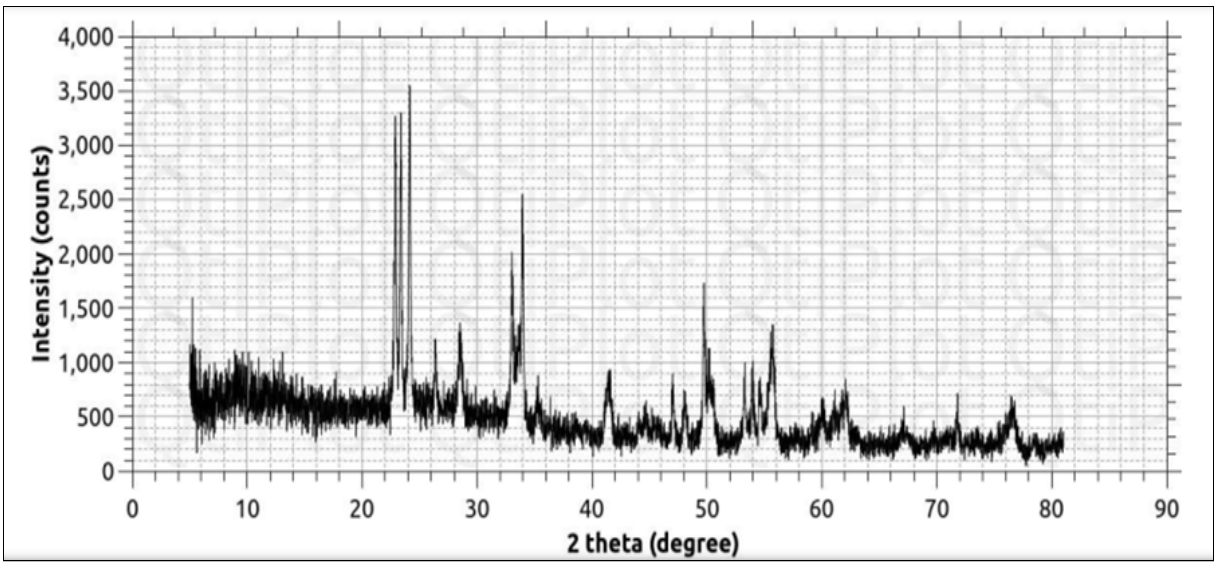

Fig 3: Representative Powder XRD pattern of annealed (doped) WO_3

Microscope analysis (FE-SEM)

These nanoparticles of tungsten oxide, both immaculate and doped, were inspected beneath the magnifying lens and are portrayed in Figure 4. Agreeing to the longer pivot, the agglomeration measure is within the extend of 1-2.5m, while the shorter hub is within the extend of 1-2m. Plates that are parallel to the substrate surface and ordinary thereto are greatly uncommon; this demonstrates that development along b-axis parallel to (020) plane is steady with the Powder XRD ponder. This gives another another piece of data. In expansion to all of this, the plates highlighted in Fig. 4 were too influenced by charge exchange between 'W' and 'O' ions. Images of strengthened unadulterated and doped WO_3-nanoparticles are appeared in Figure 5. As well as having a polydispersity character, it is additionally polygonal in shape, with a distance across of 4-5 micrometres on the level pivot and 2-3 micrometres on the longitudinal one. Amid recrystallization, particles collide at a high rate, coming about within the agglomeration of these collisions. A tempered test with superior consistency and a better crystalline nature than the unadulterated test illustrated the importance of dopants in changing the ultimate product's shape. Magnesium doped tests contain more oxygen than unadulterated tests, hence oxygen concentration could be a critical thought when attempting to redress morphological issues.

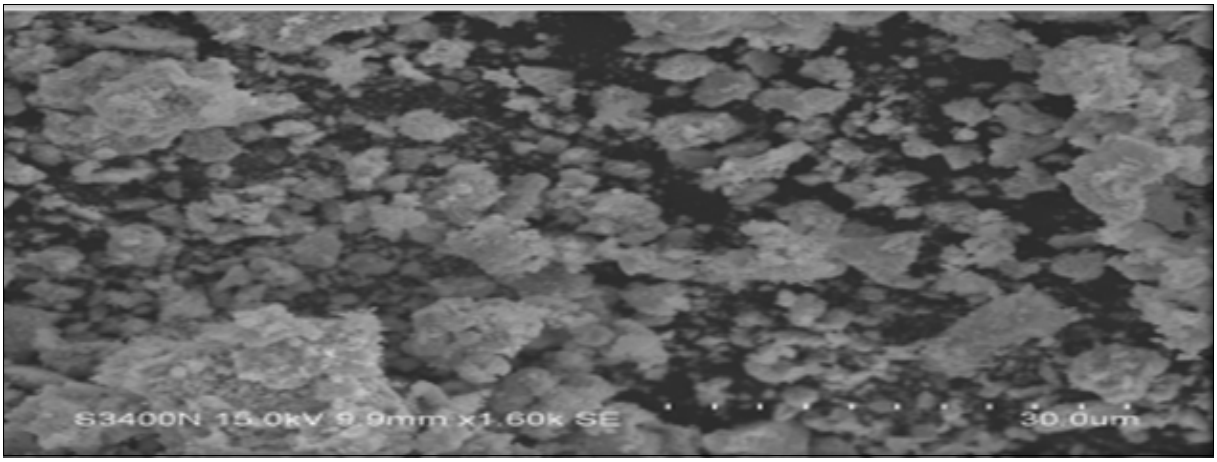

Fig 4: FE-SEM images of WO_3 .H_2O doped

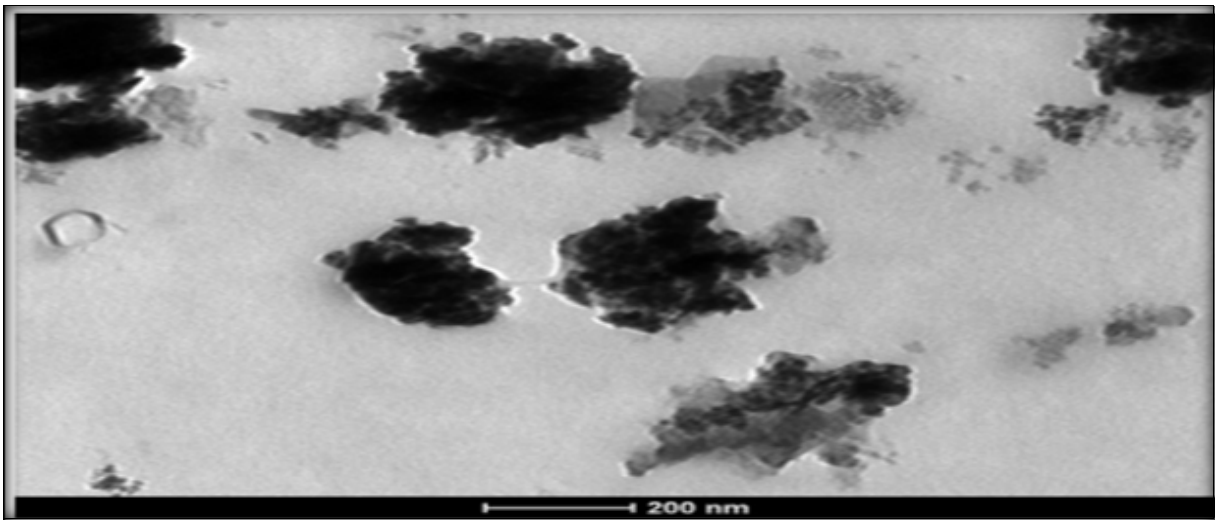

Fig 5: FE - SEM images of WO_3 doped

UV-VIS diffusion reflectance analysis (UV-VIS-DRS) Unadulterated and doped materials were considered utilizing UV -VIS diffuse reflectance spectroscopy to decide their optical characteristics. The comes about are shown in Figure 6. Within the unmistakable run, the created nanoparticles appear tall and wide reflectance crests between 500 and 650 nm, demonstrating their capacity to carry optical signals. Inside the ghostly run of 500-650 nm, the most noteworthy reflectance power appear outstanding blue and ruddy changes (as arranged tests) Kubelka-Munk (K-M show and its going with connection are given underneath) may be utilized to calculate the band hole energies for all tests.

$$\frac{K}{S} = \frac{(1-R_\infty)^2}{2R_\infty} = F(R_\infty)$$

$$R_\infty = \frac{R_{sample}}{R_{std.}}$$

F(R) is the so-called remission or Kubelka - Munk function, where

The band hole vitality Eg of the specific test is spoken to on a chart between $[F(R\infty)h\upsilon]^2$ Vs hυ. The vitality of the band crevices were decided to be 3.27 and 3.33 eV, separately, as a work of Magnesium substance. In differentiate, beneath the same doping circumstances, the band crevice energies of tempered tests were 2.87 eV and 3.44 eV. It is conceivable to clarify the increment in Eg as arranged utilizing the Burstein Greenery (BM) impact, which states that the least states within the conduction band are blocked and moves are permitted as it were to the unblocked valance level (between W^{6+} and Mg^{2+}) due to the introduction of Mg^{2+} particle within the middle of the road vitality state. For tempered tests, in any case, the rise in band hole energies with dopant concentration is due to the trade interaction between the band electrons of dx2- y2 and day orbital of tungsten to the dx2-y2, dz2, and dz2 orbitals of Mg^{2+}. It comes about in a narrowing of the band hole and a positive alteration within the valance band (Fig. 6).

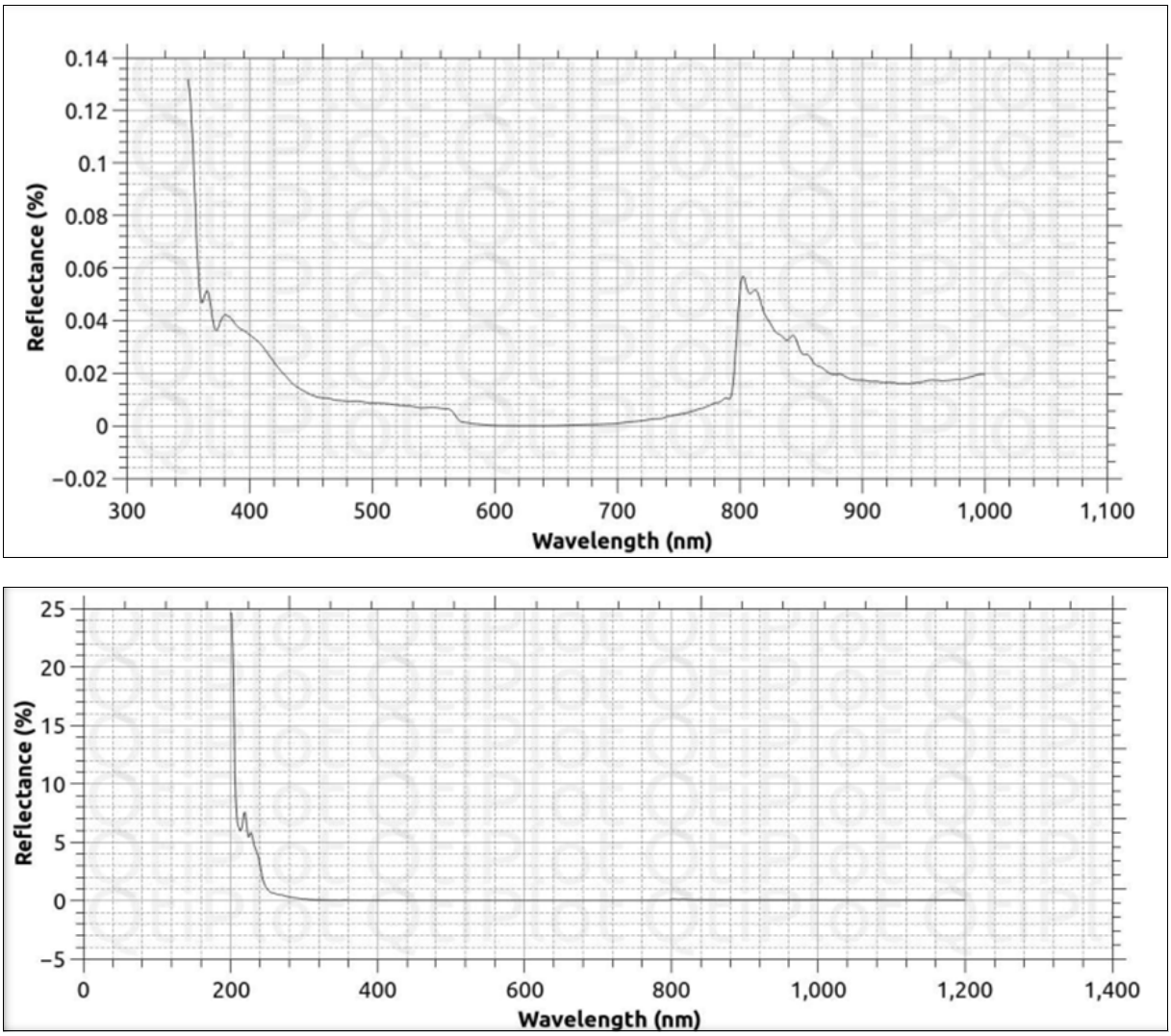

Fig. 6: UV - VIS - DRS plots of doped $WO_3.H_2O$ and WO_3

Conclusions

By utilizing a viable microwave illumination approach in a surrounding environment, we have effectively completed both immaculate and doped $WO_3.H_2O$. All of the ultimate items (Unadulterated and Doped) were found to have orthorhombic stages in their continuous crystalline stages. Powder XRD examination demonstrated that toughened tests, both unadulterated and doped (5wt. percent) tests, shaped orthorhombic structures. As a result, these shocking discoveries uncovered that dopants have a part in rectifying the wrapped up product's oxygen concentration. Ponders on UV, VIS, and DRS will give as proof.to know that the as-prepared tests have more optical conductivity than that of the strengthened tests. This perception suggests the specified optical conductivity can be attained by doping components themselves rather than the toughening prepare. The curiously comes about from hysteresis circles proposed that the doped tests attempt to continue well into long-standing time in photocatalytic applications

Reference

1. Wang N, Liu S, Zeng XT, Magdassi S, Long Y. J Mater Chem C. 2015;3(26):6771-6777.
2. Baser DS, Cheng Z, Fan JA, Fan LS. ACS Sustain Chem Eng. 2021;9(7):2651-2660.
3. Nourmohammadian M, Chharganeh Kalangestani F. Opt Quant Electron. 2023;55(1):20.
4. Zhang M, Yang Y, Han W, Li M, Ye K, Sun Y, Yan Y. J Solid State Electrochem. 2013;17:2671-2678.
5. Mohammed YH. Superlattices Microstruct. 2019;131:104-116.
6. Borghei SM, Kamali S, Shakib MH, Bazrafshan A, Ghoranneviss M. J Fusion Energy. 2011;30:433-436.
7. Kazuta M, Tanaka K. J Catal. 1990;123(1):164-172.
8. Cohen ML, Lin PJ, Roessler DM, Walker WC. *Phys Rev.* 1967;155(3):992.
9. Tajima K, Yamada Y, Bao S, Okada M, Yoshimura K. Jpn J Appl Phys. 2009;48(10R):102402.
10. Tanaka N, Kimata H, Takashima T, Kizuka T. Surf Rev Lett. 1998;5(03n04):723-729.
11. Han Y, Li S, Ding R, Xu W, Zhang G. Chin J Chem Eng. 2019;27(3):564-574.
12. Yang S, Yang F, Liao C, Li M, Wang X. J Rare Earths. 2010;28:385-388.
13. Liu XJ, Huang RS, Wang HY, Liu SH. Sci Technol Weld Join. 2007;12(3):258-260.
14. Das PS, Dey A, Mandal AK, Dey N, Mukhopadhyay AK. Surf Eng. 2016;32(1):15-20.
15. McLaughlin DF, Sessions CE, Marra JE. Nucl Technol. 1992;99(2):242-251.
16. Castrillejo Y, Martinez AM, Pardo R, Haarberg GM. Electrochim Acta. 1997;42(12):1869-1876.
17. Kaneco S, Ogawa J, Ohta K, Itoh S, Mizuno T. Talanta. 1998;46(1):139-143.
18. Ohta K, Ogawa J, Mizuno T. Fresenius J Anal Chem. 1997;357:995-997.

19. Itoh S, Kaneco S, Ohta K, Mizuno T. Anal Chim Acta. 1999;379(1-2):169-173.
20. Cheng J, Steckl AJ. J Vac Sci Technol B. 2001;19(6):2551-2554.
21. Tajima K, Yamada Y, Bao S, Okada M, Yoshimura K. Appl Phys Lett. 2007;91(5).
22. Liu Z, Li J, Peng H, Xie A, Li Z. Coatings. 2023;13(6):1087.
23. Tajima K, Yamada Y, Bao S, Okada M, Yoshimura K. J Appl Phys. 2008;103(1).
24. Jacob KT, Valderrama JN. J Solid State Chem. 1977;22(3):291-295.
25. Tajima K, Yamada Y, Okada M, Yoshimura K. Thin Solid Films. 2011;519(22):8114-8118.
26. Jaybhaye S, Shinde N, Jaybhaye S, Narayan H. J Nanotechnol Nanomater. 2022;3(2):67-76.
27. Wang Y, Wang J, Zeng Z, Liu H, He S, Hua Z. Sep Purif Technol. 2023;317:123857.
28. Zhang X, Cui J, McKeon J, Javey A, Cuevas A. ACS Appl Mater Interfaces. 2016;8(23):14671-14677.
29. Flores Gutiérrez A, Brittle S, Richardson TH, Dunbar A. *Sens Actuators B Chem.* 2014;202:854-860.
30. Sanjeev Kumar LG, Thirumalaikumarasamy D, Karthikeyan K, Mathanbabu M, Ashokkumar M, Ramachandran CS. Mater Today Proc. 2023;78:700-707.
31. Tsang M, Armutlulu A, Martinez AW, Allen SA, Allen MG. *Microsyst Nanoeng.* 2015;1(1):1-10.
32. Ezhilselvi V, Balaraju JN, Subramanian S. Surf Coat Technol. 2017;325:270-276.
33. Banerjee S, Poria S, Sutradhar G, Sahoo P. Mater Res Express. 2019;6(8):0865c6.
34. Zhang K, Hatano Y. Fusion Eng Des. 2010;85(7-9):1090-1093.
35. Peled E, Straze H. J Electrochem Soc. 1977;124(7):1030.
36. Zhou M, Shen J, Hu D, Gao R, Li S. Int J Adv Manuf Technol. 2017;92:3983-3990.
37. Abdal-Hay A, Dewidar M, Lim J, Lim JK. Ceram Int. 2014;40(1):2237-2247.
38. Jaballah S, Benamara M, Dahman H, Ly A, Lahem D, Debliquy M, El Mir L. Mater Chem Phys. 2020;255:123643.
39. Duan S, Dudley PG, Inman D. ECS Proc Volumes. 1986;1986(1):248.
40. Xu S, Li H, He Y, Yan S, Cheng X, Chen W, Yan J, Wu G, Yuan X. Vacuum. 2024;222:113031.
41. Kartsonakis IA, Balaskas AC, Koumoulos EP, Charitidis CA, Kordas G. Corros Sci. 2012;65:481-493.
42. Thirumoorthi G, Gnanavel B. Int J Nanosci. 2021;21:250042.
43. Thirumoorthi G, Gnanavel B. Int J Sci Res. 2023;242.
44. Thirumoorthi G, Gnanavel B. Int J Creat Res Thoughts. 2023;C156.